Title

Kinetically Controlled Self-Assembly of Binary Polymer-Grafted Nanocrystals into Ordered Superstructures via Solvent Vapor Annealing

Journal

Nano Letters, 21(12)

ISSN

1530-6984

Authors

Wang, Yi

Chen, Jun

Zhu, Chenhui

et al.

Publication Date

2021-06-23

DOI

10.1021/acs.nanolett.1c00890

Kinetically Controlled Self-Assembly of Binary Polymer-Grafted Nanocrystals into Ordered Superstructures via Solvent Vapor Annealing

Yi Wang[1], Jun Chen[1], Chenhui Zhu[2], Baixu Zhu[1], Soojin Jeong[1], Yi Yi[1], Yang Liu[1], Joshua Fiadorwu[3], Peng He[3], Xingchen Ye[1,*]

[1] Department of Chemistry, Indiana University, Bloomington, IN 47405, USA

[2] Advanced Light Source, Lawrence Berkeley National Laboratory, Berkeley, California 94720, USA

[3] Department of Chemistry, North Carolina Agricultural and Technical State University, Greensboro, North Carolina 27411, USA

ABSTRACT: Polymer-inorganic nanocomposites based on polymer-grafted nanocrystals (PGNCs) are enabling technologically relevant applications owing to their unique physical, chemical, and mechanical properties. While diverse PGNC superstructures have been realized through evaporation-driven self-assembly, this approach presents multifaceted challenges in experimentally probing and controlling assembly kinetics. Here, we report kinetically controlled assembly of binary superstructures from a homogeneous disordered PGNC mixture utilizing solvent vapor annealing (SVA). Using $NaZn_{13}$-type superstructure as a model system, we demonstrate that varying the solvent vapor pressure during SVA allows for exquisite control of the rate and extent of PGNC assembly, providing access to nearly complete kinetic pathways of binary PGNC crystallization. Characterization of kinetically arrested intermediates reveals that assembly follows a multistep crystallization pathway involving spinodal-like preordering of PGNCs prior to $NaZn_{13}$ nucleation. Our work opens up new avenues for the predictive synthesis of multicomponent PGNC superstructures exhibiting multifunctionality and emergent properties through thorough understanding of kinetic pathways.

Polymer-inorganic nanocomposites are enabling transformative advances in applications including photonics, plasmonics, fuel cells, photovoltaics, nanomembranes, among others.[1-6] Assemblies of polymer-grafted nanocrystals (PGNCs) represent a modular materials platform for developing functional nanocomposites with tailored properties, versatile processability and responsiveness to multiple stimuli.[2, 7-11] Grafting polymers onto pre-synthesized nanocrystals (NCs) introduces new energetic contributions arising from the conformational entropy and interaction enthalpy of polymer chains, offering a vast parameter space for nanocomposite design.[12-18] While diverse NC and PGNC superstructures have been synthesized by evaporation-driven self-assembly, [8, 19-28] it remains very challenging to study the kinetic pathways of crystallization especially for multicomponent systems. The main challenge lies in the difficulty of real-space observation of structural intermediates during disorder-to-order transitions.

Solvent vapor annealing (SVA) has been utilized extensively for controlling the morphology and ordering of polymeric materials.[29] Exposure to solvent vapors can swell the polymer chains and lower the glass transition temperature, thereby increasing chain mobility. Importantly, SVA can be performed at a constant solvent vapor pressure to provide steady thermodynamic driving force for structural evolution and be stopped on-demand to access intermediate structures. Despite its proven effectiveness, there have been very few reports of using SVA to synthesize NC and PGNC assemblies yet limiting to one-component systems.[30-33]

Herein, we describe kinetically controlled assembly of binary PGNCs into ordered phases using SVA. A homogeneous disordered mixture of PGNC film was prepared by spin-coating onto Si substrates, which was subject to SVA under a well-defined normalized solvent vapor pressure, p/p_0 (p and p_0 denote experimental and saturated solvent vapor pressure, respectively). Our custom-built SVA apparatus (Figure 1a) combines a continuous flow of saturated solvent vapors with a N_2 diluent each regulated by a mass flow controller (MFC). Fast quenching of solvent-swollen PGNC films (within 30s) allows structures evolved after different SVA durations to be preserved and characterized. Monodisperse Fe_3O_4 NCs with the core size of 5.4 nm and 13.5 nm were synthesized and functionalized with 5.5 kDa pentaethylenehexamine-terminated polystyrene (PS) and 8.2 kDa diethylenetriamine-terminated PS with an estimated grafting density of 0.81 and 0.56 chains/nm^2, respectively (Figures S1-S4, and Tables S1-S2). Both Fe_3O_4 PGNCs readily form two-dimensional hexagonal superlattices with an average center-to-center interparticle distance of 12.0 nm and 19.8 nm (Figure 1b-d), respectively, giving rise to an effective PGNC size ratio of 0.61. One of the stable phases predicted for this size ratio is $NaZn_{13}$.[8-9, 19, 28, 34]

SVA-induced disorder-to-order transition for films with a PGNC number ratio close to 13:1 was studied using scanning electron microcopy (SEM). Both top-view and cross-sectional SEM images indicated that the as-spun film consisted of a disordered, random mixture of small and large PGNCs (Figure 1e and Figure S5a-b). After SVA under 0.95 p/p_0 $CHCl_3$ vapors for 15 min, PGNCs self-assembled into micrometer-sized ordered domains with four-fold symmetry (Figure 1f-g). Transmission

electron microscopy (TEM) imaging of PGNC films prepared on mica substrates and annealed under otherwise identical conditions confirmed the formation of $NaZn_{13}$-type superstructure with a [001] preferred orientation (Figure 1h). Cross-sectional SEM image revealed that ordering persisted through the entire film thickness (Figure 1i and Figure S5g-h).

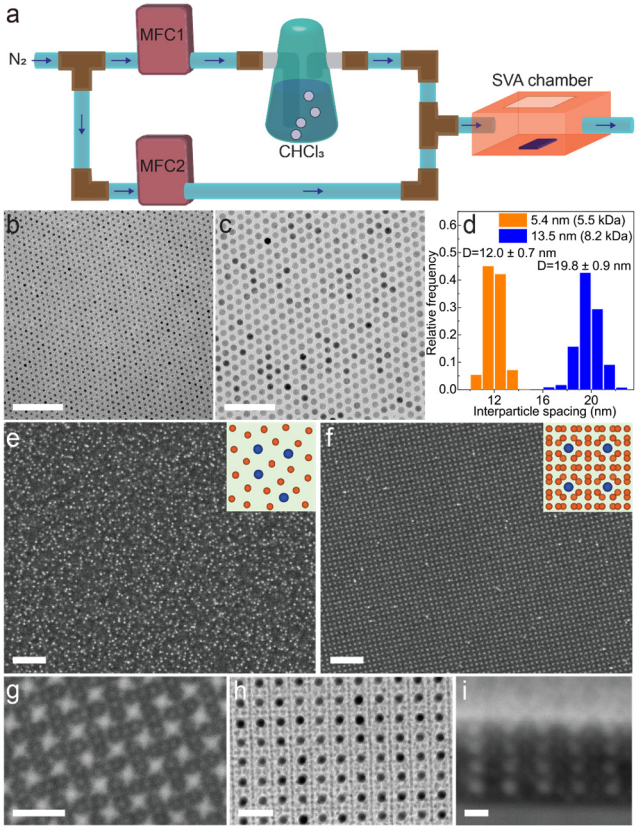

Figure 1. Formation of $NaZn_{13}$-type PGNC superstructure via SVA under 0.95 p/p_0 of $CHCl_3$ vapors. (a) Scheme of SVA setup. (b-c) TEM images of Fe_3O_4 PGNCs with the core diameter of (b) 5.4 nm and (c) 13.5 nm. (d) Histograms of center-to-center interparticle distance of PGNCs. (e-g) Representative SEM images of as-spun binary PGNC film (e) and after 15 min SVA (f-g). (h) TEM image of mica-supported binary PGNC film after 15 min SVA. (i) Cross-sectional SEM image of $NaZn_{13}$-type superstructure. Scale bars: (b-c) 100 nm, (e-f) 200 nm, (g-h) 50 nm, (i) 20 nm.

Rapid quenching of solvent-swollen films to dry state provides an unprecedented means of studying the kinetic pathways of binary PGNC superstructure formation. Figure 2 and Figure S6 show representative SEM images of PGNC films upon SVA under 0.95 p/p_0 $CHCl_3$ vapors for different durations. A homogenous disordered PGNC film was first formed by spin-coating (Figure 2a). After 2 min SVA, a microscale phase-separated state was observed with distinct regions enriched with either small or large PGNCs, reminiscent of spinodal decomposition (Figure 2b and Figure S7). The fast Fourier transform (FFT) pattern shows diffraction arcs (Figure 2b), which originates from the short-range order of small-PGNC-rich regions. After 3 min SVA, $NaZn_{13}$-type nuclei emerged with average dimensions of ~140 nm x 140 nm and an areal density of about 1 μm^{-2}, corresponding to the initial nucleation stage (Figure 2c). After 5 min SVA, the density of $NaZn_{13}$-type nuclei increased to ~10 μm^{-2} with the average domain size reaching nearly 200 nm x 200 nm, indicating continuous nucleation without rapid grain growth (Figure 2d and Figure S8). The FFT pattern shows four-fold diffraction peaks arising from $NaZn_{13}$-type domains. From 5 to 10 min, the $NaZn_{13}$ domain size continued to increase with a concomitant reduction in domain density, corresponding to a coarsening/ripening stage where independently nucleated domains consolidated by removing grain boundaries (Figure 2e). After 15 min SVA, highly crystalline $NaZn_{13}$ superstructures formed with the majority of point defects and grain boundaries observed in the previous stage annealed out, as seen from SEM images and the sharp and higher-order diffraction spots in the FFT pattern (Figure 2f). Formation of $NaZn_{13}$-type superstructures appeared to be robust against modest off-stoichiometries between small and large PGNCs and variations in the initial film thickness, provided that the thickness exceeded a certain threshold (Figures S9-S10).

To complement real-space electron microscopy imaging of local structures, grazing incidence small-angle X-ray scattering (GISAXS) was employed to obtain statistically averaged information of structural order and lattice parameters. The GISAXS pattern of as-spun film displayed no Bragg diffraction peak (Figure 2g), in agreement with its disordered structure. By contrast, multiple diffraction peaks were observed on the GISAXS pattern of PGNC films after 15 min SVA, which can be indexed to the [001]-oriented $NaZn_{13}$ phase (Figure 2h). The retrieved out-of-plane lattice constant is 45.0 nm, that is 79% of the in-plane lattice constant (57.1 nm), suggesting a lattice contraction normal to the Si substrate. We attribute this vertical contraction to the rapid deswelling of PGNC films. Similar phenomena have been observed in other soft matter assemblies including block copolymer films and alkyl-ligand-coated NC films.[20-21, 35-36] Furthermore, horizontal linecuts near the Yoneda peak revealed that development of $NaZn_{13}$-type crystalline order preceded superstructure densification to attain the final lattice constants (Figure 2i).

To develop a quantitative understanding of the effects of solvent vapor pressure on the assembly behavior of binary PGNCs, we monitored film thickness in-situ using a spectroscopic reflectometer. A typical film swelling curve consists of a fast build-up step followed by steady-state swelling and rapid deswelling to dry state within 30s (Figure 3a). When the relative flow rate of saturated solvent vapor and N_2 diluent was varied from 93/7, 85/15, 78/22 to 68/32, the solvent vapor pressure inside the SVA chamber changed from 0.95, 0.88, 0.83 to 0.74 p/p_0 (Detailed calculations are provided in the Supporting Information). To validate our SVA setup, the thickness of a pure polystyrene film under different p/p_0 was measured to obtain the polymer volume fraction, φ_p, and the data were fitted using the Flory-Huggins equation: [37]

$$\ln\left(\frac{p}{p_0}\right)=\chi_{P,S}\varphi_p^2+\ln\left(1-\varphi_p\right)+\left(1-\frac{1}{N}\right)\varphi_p \qquad (1)$$

N is degree of polymerization and $\chi_{P,S}$ is the Flory-Huggins interaction parameter. The retrieved $\chi_{P,S}$ for PS/$CHCl_3$

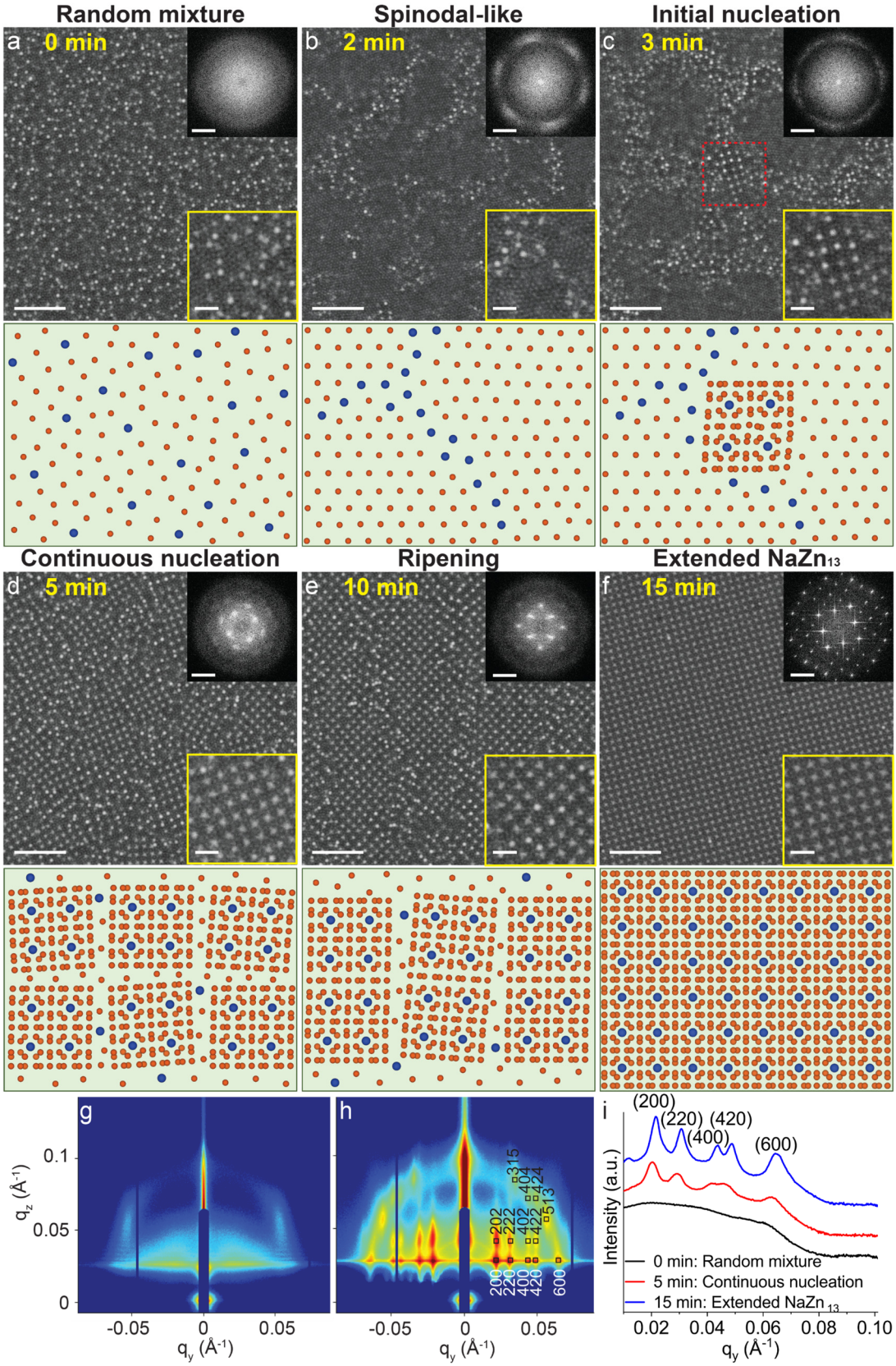

Figure 2. Structure evolution of a disordered mixture of PGNCs to $NaZn_{13}$-type superstructure under 0.95 p/p_0 of $CHCl_3$ vapors. (a-f) Low-magnification SEM image and schematic structure (main image and below), high-magnification SEM image (bottom inset), corresponding FFT pattern (top inset) of PGNC films (a) before and (b-f) after SVA for (b) 2 min, (c) 3 min, (d) 5 min, (e) 10 min and (f) 15 min. Scale bars: (main SEM images) 200 nm, (inset SEM images) 50 nm, (FFT patterns) 0.05 nm^{-1}. (g-h) GISAXS patterns of PGNC films (g) before and (h) after 15 min SVA. (i) Horizontal line profile of the GISAXS pattern along q_z = 0.031 $Å^{-1}$ for as-spun PGNC films and films after SVA for 5 min and 15 min.

is 0.3, in agreement with previous literature reports.[38] The volume fraction of PGNCs (φ_{PGNC}) in swollen films can be estimated as $\varphi_{PGNC} = d_0/d_{sw}$ (d_0 and d_{sw} are dry and swollen film thicknesses, respectively). When p/p_0 was reduced from 0.95 to 0.88, 0.83 and 0.74, φ_{PGNC} increased from 0.44 to 0.54, 0.61 and 0.69 (Figure 3b). We attribute the higher φ_{PGNC} values than φ_P under identical p/p_0 to the non-swollen PGNC cores and different conformations between polymer brushes on PGNCs and free polymers.

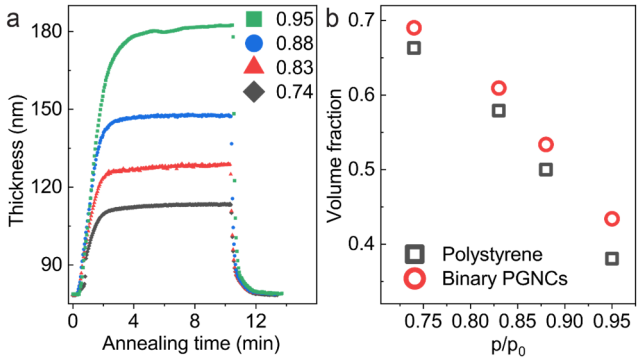

Figure 3. (a) The thickness profile of binary PGNC films during SVA under different p/p_0. (b) Volume fraction of 190 kDa unfunctionalized PS and binary PGNCs as a function of p/p_0.

The solvent vapor pressure or φ_{PGNC}, was found to play a dominant role in determining assembly kinetics. As shown in the "time-solvent vapor pressure-transformation" diagram (Figure 4 and Figure S11), no superstructure was formed after prolonged SVA for 5h at 0.74 p/p_0. The PGNC film simply swelled (up to 145% of its original thickness) and deswelled without particle reorganization. This suggests that at such a high volume fraction (φ_{PGNC}=0.69), nucleation is severely hampered likely because of retarded PGNC diffusion. In the intermediate vapor pressure regime (e.g., 0.83 p/p_0), spinodal-like preordering of small PGNCs was observed after SVA for 15 min (Figure 4 and Figure S12), whereas only sparsely distributed small $NaZn_{13}$-type domains (~140 nm x 140 nm, ~0.3 μm^{-2}) resulted after 1.5h SVA. Therefore, nucleation barrier of $NaZn_{13}$ is still high under such conditions and grain growth is essentially suppressed. At 0.88 p/p_0, extended $NaZn_{13}$ domains were obtained after 40 min SVA, although assembly kinetics was slower than that at 0.95 p/p_0 (Figure 4 and Figure S13). Collectively, nucleation and growth of $NaZn_{13}$-type PGNC superstructures only become kinetically facile when φ_{PGNC} lies within the range of 0.44 to 0.54. The fact that lower φ_{PGNC} resulted in faster assembly kinetics in the high-vapor-pressure regime suggests that crystallization is limited by the diffusion dynamics of PGNCs rather than thermodynamic preference.

The softness of PGNCs plays important roles in dictating the kinetic pathways of superstructure formation. Of note, the range of φ_{PGNC} (~0.44-0.54) amenable to $NaZn_{13}$ crystallization is lower than theoretical predictions or previous studies on hard-sphere colloids.[39-40] For instance, a recent report of event-driven molecular dynamic simulations demonstrated that $NaZn_{13}$-type binary hard-sphere crystals could grow directly from the fluid phase at particle volume fractions of φ~0.565-0.590.[40] In a pioneering study on $NaZn_{13}$ formation in suspensions of nearly hard-sphere particles, a range of φ~0.512-0.553 was experimentally determined.[39] Our results indicate that distinct from colloidal hard-sphere systems, crystallization of binary PGNCs into superstructures can be feasible over a broader range of φ with a substantially lower onset. At a constant φ_{PGNC} of 0.44, the assembly kinetics slowed down when increasing NC core size or decreasing PS length, yet still following the same assembly pathway (Figure S14-S17). Such softness-enhanced crystallization of binary phases was recently demonstrated using computer simulations.[41-42] Furthermore, our observation of spinodal-like preordering of PGNCs prior to $NaZn_{13}$ nucleation cannot be accounted for by the classical nucleation theory where nuclei having the same density and symmetry as the stable solid directly emerge from the liquid phase.[43] Instead, a multistep crystallization pathway was clearly at play, which has been increasingly recognized in various colloidal systems both experimentally and through simulations.[43-45]

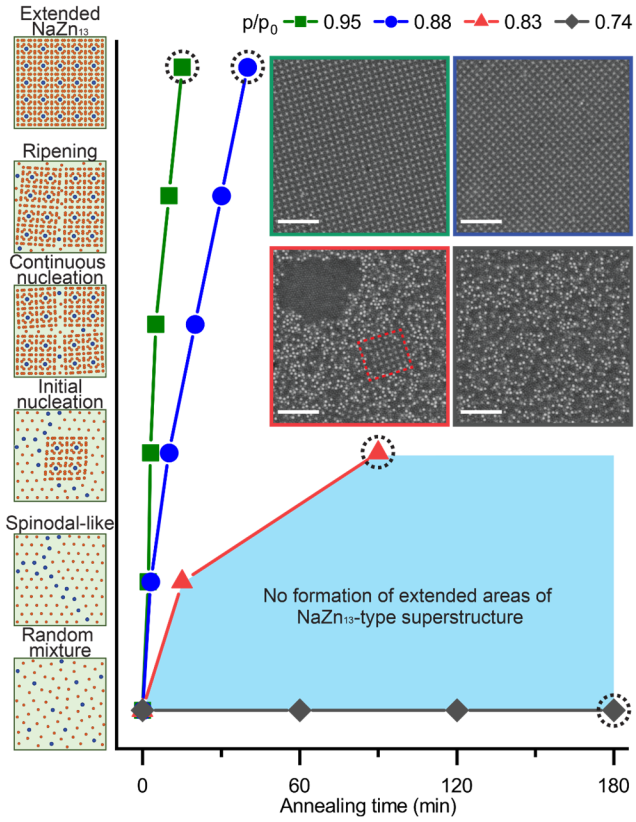

Figure 4. Time-solvent vapor pressure-transformation diagram of binary PGNCs undergoing $CHCl_3$ SVA. SEM images show typical film morphologies at late stages (as indicated by dotted circles) after SVA under different p/p_0. Scale bars: 200 nm.

In conclusion, we show that using SVA, the structural evolution of a homogeneous disordered mixture of PGNCs to ordered superstructures can be halted on-demand and analyzed in detail. We establish that controlling the solvent vapor pressure during SVA allows for exquisite control over the rate and extent of PGNC assembly. Analysis of kinetically arrested intermediates uncovers that crystallization of $NaZn_{13}$-type superstructures follows a multistep crystallization pathway involving spinodal-like preordering of small PGNCs prior to $NaZn_{13}$ nucleation, and development of $NaZn_{13}$-type order precedes superstructure densification. Our work not only provides an effective means of forming multicomponent PGNC superstructures, but also opens the door for understanding and ultimately controlling the kinetic pathways and superstructure selections for PGNC assemblies.

ASSOCIATED CONTENT

Supporting Information. Experimental details; Materials characterization of polymers and PGNCs; Additional SEM and TEM images of PGNC films after SVA under different p/p_0.
This material is available free of charge via the Internet at http://pubs.acs.org.

AUTHOR INFORMATION

Corresponding Author

*xingye@indiana.edu.

Funding Sources

This work was supported by the start-up fund from Indiana University. P.H. and J.F acknowledge support from the Indiana University-Minority Serving Institutions STEM Summer Scholars Institute program and College of Science and Technology at North Carolina Agricultural and Technical State University. This research also made use resources at the Advanced Light Source of Lawrence Berkeley National Laboratory, which is a DOE Office of Science User Facility supported under contract no. DE-AC02-05CH11231.

Notes

The authors declare no competing financial interest.

ACKNOWLEDGMENT

We thank Indiana University Nanoscale Characterization Facility and Electron Microscopy Center for access of instrumentation.

REFERENCES

(1) Kumar, S. K.; Benicewicz, B. C.; Vaia, R. A.; Winey, K. I. 50th Anniversary Perspective: Are Polymer Nanocomposites Practical for Applications? *Macromolecules* **2017,** *50*, 714-731.

(2) Fernandes, N. J.; Koerner, H.; Giannelis, E. P.; Vaia, R. A. Hairy Nanoparticle Assemblies as One-Component Functional Polymer Nanocomposites: Opportunities and Challenges. *MRS Commun.* **2013,** *3*, 13-29.

(3) Gao, B.; Arya, G.; Tao, A. R. Self-Orienting Nanocubes for the Assembly of Plasmonic Nanojunctions. *Nat. Nanotechnol.* **2012,** *7*, 433-437.

(4) Kao, J.; Thorkelsson, K.; Bai, P.; Zhang, Z.; Sun, C.; Xu, T. Rapid Fabrication of Hierarchically Structured Supramolecular Nanocomposite Thin Films in One Minute. *Nat. Commun.* **2014,** *5*, 4053.

(5) Pastoriza-Santos, I.; Kinnear, C.; Pérez-Juste, J.; Mulvaney, P.; Liz-Marzán, L. M. Plasmonic Polymer Nanocomposites. *Nat. Rev. Mater.* **2018,** *3*, 375-391.

(6) Mueller, N. S.; Okamura, Y.; Vieira, B. G. M.; Juergensen, S.; Lange, H.; Barros, E. B.; Schulz, F.; Reich, S. Deep Strong Light–Matter Coupling in Plasmonic Nanoparticle Crystals. *Nature* **2020,** *583*, 780-784.

(7) Akcora, P.; Liu, H.; Kumar, S. K.; Moll, J.; Li, Y.; Benicewicz, B. C.; Schadler, L. S.; Acehan, D.; Panagiotopoulos, A. Z.; Pryamitsyn, V.; Ganesan, V.; Ilavsky, J.; Thiyagarajan, P.; Colby, R. H.; Douglas, J. F. Anisotropic Self-Assembly of Spherical Polymer-Grafted Nanoparticles. *Nat. Mater.* **2009,** *8*, 354-359.

(8) Ye, X.; Zhu, C.; Ercius, P.; Raja, S. N.; He, B.; Jones, M. R.; Hauwiller, M. R.; Liu, Y.; Xu, T.; Alivisatos, A. P. Structural Diversity in Binary Superlattices Self-Assembled from Polymer-Grafted Nanocrystals. *Nat. Commun.* **2015,** *6*, 10052.

(9) Boles, M. A.; Engel, M.; Talapin, D. V. Self-Assembly of Colloidal Nanocrystals: From Intricate Structures to Functional Materials. *Chem. Rev.* **2016,** *116*, 11220-11289.

(10) Chancellor, A. J.; Seymour, B. T.; Zhao, B. Characterizing Polymer-Grafted Nanoparticles: From Basic Defining Parameters to Behavior in Solvents and Self-Assembled Structures. *Anal. Chem.* **2019,** *91*, 6391-6402.

(11) Yi, C.; Yang, Y.; Liu, B.; He, J.; Nie, Z. Polymer-Guided Assembly of Inorganic Nanoparticles. *Chem. Soc. Rev.* **2020,** *49*, 465-508.

(12) Dukes, D.; Li, Y.; Lewis, S.; Benicewicz, B.; Schadler, L.; Kumar, S. K. Conformational Transitions of Spherical Polymer Brushes: Synthesis, Characterization, and Theory. *Macromolecules* **2010,** *43*, 1564-1570.

(13) Choi, J.; Dong, H.; Matyjaszewski, K.; Bockstaller, M. R. Flexible Particle Array Structures by Controlling Polymer Graft Architecture. *J. Am. Chem. Soc.* **2010,** *132*, 12537-12539.

(14) Ehlert, S.; Taheri, S. M.; Pirner, D.; Drechsler, M.; Schmidt, H. W.; Forster, S. Polymer Ligand Exchange to Control Stabilization and Compatibilization of Nanocrystals. *ACS Nano* **2014,** *8*, 6114-6122.

(15) Zhang, J.; Santos, P. J.; Gabrys, P. A.; Lee, S.; Liu, C.; Macfarlane, R. J. Self-Assembling Nanocomposite Tectons. *J. Am. Chem. Soc.* **2016,** *138*, 16228-16231.

(16) Lenart, W. R.; Hore, M. J. A. Structure–Property Relationships of Polymer-Grafted Nanospheres for Designing Advanced Nanocomposites. *Nano-Struct. Nano-Objects* **2018,** *16*, 428-440.

(17) Yun, H.; Lee, Y. J.; Xu, M.; Lee, D. C.; Stein, G. E.; Kim, B. J. Softness- and Size-Dependent Packing Symmetries of Polymer-Grafted Nanoparticles. *ACS Nano* **2020,** *14*, 9644-9651.

(18) Yan, J.; Bockstaller, M. R.; Matyjaszewski, K. Brush-Modified Materials: Control of Molecular Architecture, Assembly Behavior, Properties and Applications. *Prog. Polym. Sci.* **2020,** *100*, 101180.

(19) Shevchenko, E. V.; Talapin, D. V.; Kotov, N. A.; O'Brien, S.; Murray, C. B. Structural Diversity in Binary Nanoparticle Superlattices. *Nature* **2006,** *439*, 55-59.

(20) Friedrich, H.; Gommes, C. J.; Overgaag, K.; Meeldijk, J. D.; Evers, W. H.; de Nijs, B.; Boneschanscher, M. P.; de Jongh, P. E.; Verkleij, A. J.; de Jong, K. P.; van Blaaderen, A.; Vanmaekelbergh, D. Quantitative Structural Analysis of Binary Nanocrystal Superlattices by Electron Tomography. *Nano Lett.* **2009,** *9*, 2719-2724.

(21) Smith, D. K.; Goodfellow, B.; Smilgies, D. M.; Korgel, B. A. Self-Assembled Simple Hexagonal AB_2 Binary Nanocrystal Superlattices: SEM, GISAXS, and Defects. *J. Am. Chem. Soc.* **2009,** *131*, 3281-3290.

(22) Dong, A.; Chen, J.; Vora, P. M.; Kikkawa, J. M.; Murray, C. B. Binary Nanocrystal Superlattice Membranes Self-Assembled at the Liquid-Air Interface. *Nature* **2010,** *466*, 474-477.

(23) Singh, G.; Chan, H.; Baskin, A.; Gelman, E.; Repnin, N.; Král, P.; Klajn, R. Self-Assembly of Magnetite Nanocubes into Helical Superstructures. *Science* **2014,** *345*, 1149.

(24) Wei, J.; Schaeffer, N.; Pileni, M. P. Ligand Exchange Governs the Crystal Structures in Binary Nanocrystal Superlattices. *J. Am. Chem. Soc.* **2015,** *137*, 14773-14784.

(25) Weidman, M. C.; Smilgies, D. M.; Tisdale, W. A. Kinetics of the Self-Assembly of Nanocrystal Superlattices Measured by Real-Time in Situ X-Ray Scattering. *Nat. Mater.* **2016,** *15*, 775-781.

(26) Wang, Z.; Bian, K.; Nagaoka, Y.; Fan, H.; Cao, Y. C. Regulating Multiple Variables to Understand the Nucleation and Growth and Transformation of PbS Nanocrystal Superlattices. *J. Am. Chem. Soc.* **2017,** *139*, 14476-14482.

(27) Nagaoka, Y.; Tan, R.; Li, R.; Zhu, H.; Eggert, D.; Wu, Y. A.; Liu, Y.; Wang, Z.; Chen, O. Superstructures Generated from Truncated Tetrahedral Quantum Dots. *Nature* **2018,** *561*, 378-382.

(28) Coropceanu, I.; Boles, M. A.; Talapin, D. V. Systematic Mapping of Binary Nanocrystal Superlattices: The Role of Topology in Phase Selection. *J. Am. Chem. Soc.* **2019,** *141*, 5728-5740.

(29) Sinturel, C.; Vayer, M.; Morris, M.; Hillmyer, M. A. Solvent Vapor Annealing of Block Polymer Thin Films. *Macromolecules* **2013,** *46*, 5399-5415.

(30) Bian, K.; Choi, J. J.; Kaushik, A.; Clancy, P.; Smilgies, D. M.; Hanrath, T. Shape-Anisotropy Driven Symmetry Transformations in Nanocrystal Superlattice Polymorphs. *ACS Nano* **2011,** *5*, 2815-2823.

(31) Zhang, J.; Luo, Z.; Martens, B.; Quan, Z.; Kumbhar, A.; Porter, N.; Wang, Y.; Smilgies, D. M.; Fang, J. Reversible Kirkwood-Alder Transition Observed in Pt_3Cu_2 Nanoctahedron Assemblies under Controlled Solvent Annealing/Drying Conditions. *J. Am. Chem. Soc.* **2012,** *134*, 14043-14049.

(32) Rupich, S. M.; Castro, F. C.; Irvine, W. T.; Talapin, D. V. Soft Epitaxy of Nanocrystal Superlattices. *Nat. Commun.* **2014,** *5*, 5045.

(33) Chen, J.; Fasoli, A.; Cushen, J. D.; Wang, L.; Ruiz, R. Self-Assembly and Directed Assembly of Polymer Grafted Nanocrystals via Solvent Annealing. *Macromolecules* **2017,** *50*, 9636-9646.

(34) Travesset, A. Soft Skyrmions, Spontaneous Valence and Selection Rules in Nanoparticle Superlattices. *ACS Nano* **2017,** *11*, 5375-5382.

(35) Bosworth, J. K.; Paik, M. Y.; Ruiz, R.; Schwartz, E. L.; Huang, J. Q.; Ko, A. W.; Smilgies, D. M.; Black, C. T.; Ober, C. K. Control of Self-Assembly of Lithographically Patternable Block Copolymer Films. *ACS Nano* **2008,** *2*, 1396-1402.

(36) Hanrath, T.; Choi, J. J.; Smilgies, D. M. Structure/Processing Relationships of Highly Ordered Lead Salt Nanocrystal Superlattices. *ACS Nano* **2009,** *3*, 2975-2988.

(37) Flory, P. J. *Principles of Polymer Chemistry, 3rd Edition;* Cornell University Press: Ithaca, 1989.

(38) Knoll, A.; Magerle, R.; Krausch, G. Phase Behavior in Thin Films of Cylinder-Forming ABA Block Copolymers: Experiments. *J. Chem. Phys.* **2004,** *120*, 1105-1116.

(39) Bartlett, P.; Ottewill, R. H.; Pusey, P. N. Superlattice Formation in Binary Mixtures of Hard-Sphere Colloids. *Phys. Rev. Lett.* **1992,** *68*, 3801-3804.

(40) Bommineni, P. K.; Klement, M.; Engel, M. Spontaneous Crystallization in Systems of Binary Hard Sphere Colloids. *Phys. Rev. Lett.* **2020,** *124*, 218003.

(41) LaCour, R. A.; Adorf, C. S.; Dshemuchadse, J.; Glotzer, S. C. Influence of Softness on the Stability of Binary Colloidal Crystals. *ACS Nano* **2019,** *13*, 13829-13842.

(42) Dasgupta, T.; Coli, G. M.; Dijkstra, M. Tuning the Glass Transition: Enhanced Crystallization of the Laves Phases in Nearly Hard Spheres. *ACS Nano* **2020,** *14*, 3957-3968.

(43) Russo, J.; Tanaka, H. Nonclassical Pathways of Crystallization in Colloidal Systems. *MRS Bull.* **2016,** *41*, 369-374.

(44) De Yoreo, J. J.; Gilbert, P. U.; Sommerdijk, N. A.; Penn, R. L.; Whitelam, S.; Joester, D.; Zhang, H.; Rimer, J. D.; Navrotsky, A.; Banfield, J. F.; Wallace, A. F.; Michel, F. M.; Meldrum, F. C.; Colfen, H.; Dove, P. M. Crystallization by Particle Attachment in Synthetic, Biogenic, and Geologic Environments. *Science* **2015,** *349*, aaa6760.

(45) Ou, Z.; Wang, Z.; Luo, B.; Luijten, E.; Chen, Q. Kinetic Pathways of Crystallization at the Nanoscale. *Nat. Mater.* **2020,** *19,* 450-455.

Insert Table of Contents artwork here